Title

Combining Mass Spectrometry of Picoliter Samples with a Multicompartment Electrodynamic Trap for Probing the Chemistry of Droplet Arrays

Journal

Analytical Chemistry, 92(17)

ISSN

0003-2700

Authors

Willis, Megan D

Rovelli, Grazia

Wilson, Kevin R

Publication Date

2020-09-01

DOI

10.1021/acs.analchem.0c02343

Combining mass spectrometry of picoliter samples with a multi-compartment electrodynamic trap for probing the chemistry of droplet arrays

Megan D. Willis, Grazia Rovelli, and Kevin R. Wilson*

Chemical Sciences Division, Lawrence Berkeley National Laboratory, 1 Cyclotron Road, Berkeley, CA, USA, 94720

E-mail: krwilson@lbl.gov

Abstract

Single droplet levitation provides contactless access to the microphysical and chemical properties of micron-sized samples. Most applications of droplet levitation to chemical and biological systems use non-destructive optical techniques to probe droplet properties. To provide improved chemical specificity, we couple a multi-compartment quadrupole electrodynamic trap (QET) to single droplet mass spectrometry. Our QET continuously traps a monodisperse droplet population (∼10's – 100's of droplets), and allows for simultaneous sizing of a single droplet using its Mie scattering pattern. Single droplets are subsequently ejected to the ionization region of an ambient pressure inlet mass spectrometer. We optimize two complementary soft ionization techniques for picoliter aqueous droplets: paper spray (PS) ionization and thermal desorption glow discharge (TDGD) ionization. Both techniques detect oxygenated organic acids in single droplets with signal-to-noise ratios >100 and detection limits on the order of

10 pg. Sensitivity and reproducibility across single droplets is driven by the droplet deposition location and spray stability in PS-MS, and by ionization region humidity and analyte evaporation rate in TDGD-MS. Importantly, analyte evaporation rate can control TDGD-MS quantitative capability because high evaporation rates result in significant ion suppression. This effect is mitigated by optimizing vaporization temperature, droplet size range and analyte volatility. We demonstrate quantitative and reproducible measurements with a droplet internal standard (<10% RSD), and compare the sensitivity of PS-MS and TDGD-MS. Finally, we demonstrate application of QET-MS to studying heterogeneous chemical kinetics, with the reaction of gas phase O_3 and aqueous maleic acid droplets.

Single droplet levitation has become a widely used approach to study the microphysical properties of micron-sized samples, with applications in atmospheric and biological chemistry, and industrial and pharmaceutical processes[1–3]. This family of techniques, including electrodynamic traps of varying geometries, optical and acoustic levitation, provides significant insight into particle properties, such as volatility[4], hygroscopicity[5,6], pH[7,8], viscosity[9–11], morphology[12,13], and optical properties[14]. These approaches allow contactless access to condensed phase chemistry under controlled environmental conditions. In atmospheric applications, stable trapping over long reaction timescales can provide access to a wide range of oxidant concentrations and atmospherically relevant reaction conditions[15]. Further, droplet levitation allows access to supersaturated and highly concentrated solutions, with fine control of droplet composition by varying environmental conditions. In biological applications, droplet levitation provides small sample volumes without loss of material by adsorption to surfaces[16].

Reactive transformations in levitated droplets have largely been investigated with non-destructive optical probes[15,17–23]. While functional group information is available from Raman spectroscopy, it cannot always provide specific information on the composition of a droplet undergoing chemical transformations. Coupling measures of droplet microphysical

and optical properties with chemically specific characterization by mass spectrometry (MS) will provide a more complete mechanistic understanding of droplet reactions. A range of ambient pressure ionization techniques have been used to measure the composition of levitated droplets, with approaches differing in the size of measured droplets (diameters from micrometers to millimeters), and the method of droplet delivery into the ion source (trapped, free falling, or deposited on a substrate). We limit our discussion to analysis of levitated particles and droplets, and do not include MS analysis of single ambient atmospheric particles or their proxies, which is reviewed elsewhere[24,25].

Millimeter-sized, acoustically levitated droplets have been characterized with a wide range of ionization techniques directly during levitation of microliter droplets. These include variants of matrix-assisted laser desorption ionization (MALDI)[16,26–28], direct analysis in real time (DART) ionization[29], and field induced droplet ionization (FIDI)[30]. Both DART and FIDI have been used to follow reactive transformations in levitated droplets[29–31], though sequential measurements made on a single levitated droplet can significantly perturb its properties. Despite the utility of acoustic levitation coupled to MS for microliter droplets, micron-sized (picoliter) droplets are desirable for their smaller sample volumes and higher surface area to volume ratios. QETs can trap a wide range of droplet sizes, from 100's of nanometers to $\sim$100 microns[32,33], but the high electric field strengths and much smaller analyte masses mean that droplets must first be ejected before MS analysis and sampled completely.

Both offline and online approaches have been used with a variety of ambient ionization techniques to detect micron-sized droplets. MALDI-MS was used to detect droplets ejected from a double-ring electrodynamic balance onto a substrate, representing a contactless means of preparing small, concentrated samples[34,35]. However, this offline approach is not ideal for following reactive processes, where the gap between sample preparation and analysis could introduce bias into reaction monitoring. Free-falling picoliter droplets, generated by a droplet-on-demand dispenser, have been analyzed either singly or in groups

by electrospray-type techniques. Methanol droplets were reproducibly analyzed by a single droplet electrospray process when free-falling droplets impacted a needle carrying high voltage[36]. However, experimental challenges arise with this approach when applied to water droplets because of their higher surface tension than methanol. Aqueous droplets, free-falling onto a paper substrate, have been quantitatively analyzed with paper spray ionization MS[37]. This work demonstrated the quantitative capabilities of paper spray for droplets containing a range of analytes with limits of detection for citric acid on the order of 0.5 pg.

Two ambient ionization approaches have been applied to online detection of single, micron-sized levitated droplets. First, pure organic droplets from a double ring electrodynamic balance were detected by thermal desorption coupled to atmospheric pressure chemical ionization MS, and applied to follow the evaporation of polyethylene glycol[38]. This approach was used to determine the vapour pressure of butenedial in aqueous droplets and the impact of salts on gas-particle partitioning[39]; however, the applicability of this method was limited by significant uncertainties in the measurements. Second, aqueous droplets from a branched quadrupole trap were detected by paper spray ionization MS, demonstrating the qualitative capabilities of this approach for detecting single trapped droplets[40]. This approach was used to qualitatively identify reaction products formed in droplet merging experiments, where merged droplets contained $\sim$1 ng of material.

Chemical kinetic analysis of reactive, picoliter-volume systems requires high precision and sensitive droplet detection methods, with an ionization scheme that is well characterized to account for potential matrix effects in complex systems. A single droplet MS method both fulfilling these requirements and directly coupled to droplet levitation has not yet been demonstrated, and direct comparison between single droplet detection approaches is lacking. In this work, we couple a multi-compartment electrodynamic trap to mass spectrometry using two ambient ionization approaches amenable to aqueous droplets. We show that both helium glow discharge and paper spray ionization provide reproducible and quantitative measurements, and highlight the benefits and limitations of these two complementary tech-

niques in aqueous organic acid systems. We also demonstrate application of glow discharge ionization to following multiphase reaction kinetics, with the reaction of gas phase ozone and aqueous maleic acid.

Experimental

Quadrupole Electrodynamic Trap

The quadrupole electrodynamic trap (QET) confines charged droplets along the axis of the quadrupole trapping electrodes[40,41]. Aqueous micron-sized droplets are generated with a piezoelectric droplet dispenser (Microfab, Inc., MJ-ABP-01, with 30 µm or 50 µm orifice), and are introduced into the QET branch (Figure 1a). The droplet dispenser is driven by pulses with width $\sim 20 - 50$ µs and amplitude up to 50 V.

During droplet generation at the dispenser, a voltage is applied to an induction electrode ($\pm$ 100 – 500 V) to induce a net charge on the droplet. Charged droplets are confined in the electric field generated by the four quadruople stainless steel trapping electrodes, with an AC amplitude of $\sim$100 – 500 V and frequency of 100 – 500 Hz. Droplets fall approximately 12 cm within a humidity controlled gas flow to the lower portion of the QET where they are held with a balancing electrode, using the design described in Jacobs et al.[40]. A static DC voltage (up to $\pm$ 500 V) is applied to the balancing electrode to allow contactless droplet levitation.

The QET allows levitation of multiple droplets, facilitating time resolved experiments with a simultaneously produced droplet population of consistent size (variability in diameter on the order of $\pm$2.5%) and chemical composition. Two, or more, sets of balancing electrodes (4 thin metal fins, positioned between the QET rods) are fixed approximately 6 cm apart along the lower portion of the QET providing multiple compartments for droplet trapping (Figure 1a). A population of droplets is dispensed through the QET branch at constant droplet dispenser voltage and pulse width, and trapped in the upper compartment (tens

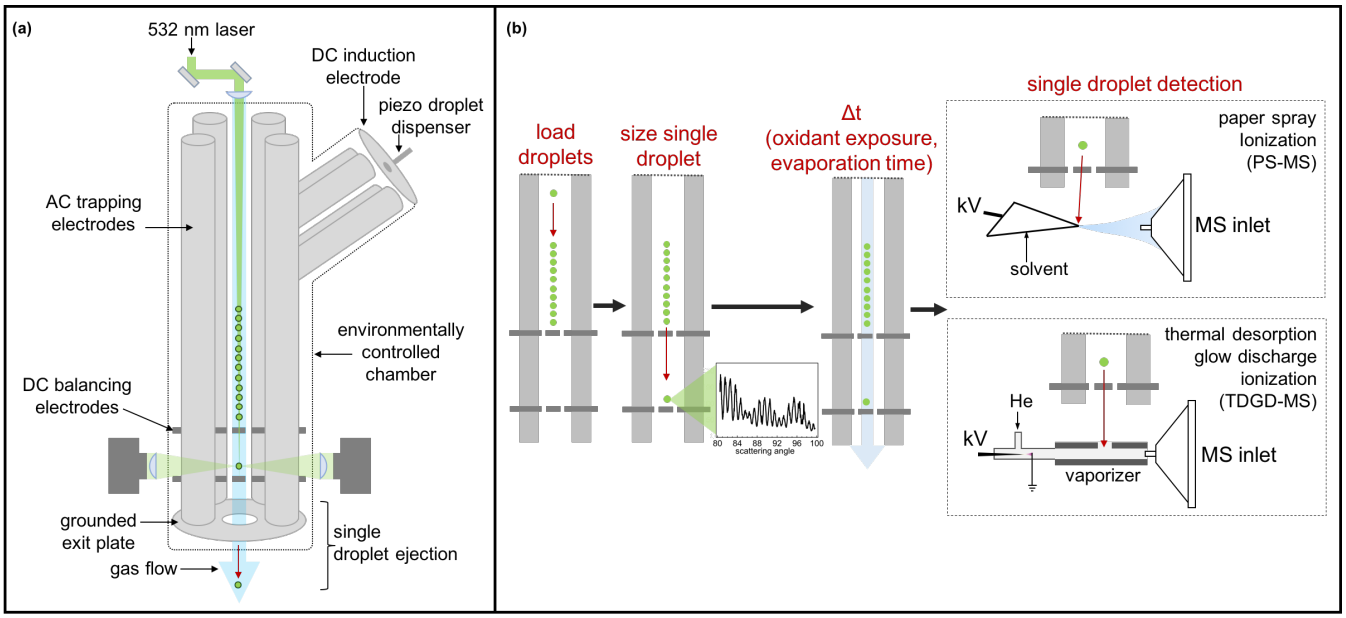

Figure 1: (a) Schematic of the multi-compartment quadrupole electrodynamic trap (QET). (b) Schematic of the experimental sequence. A population of droplets is first loaded into the QET, then a single droplet is extracted into the lower compartment for sizing. Single droplets can successively be directly ejected for analysis by single droplet mass spectrometry, or trapped under a specific environmental condition for a period of time before analysis. Sizing of a single droplet in the lower compartment occurs continuously during reactions or evaporation.

to hundreds of droplets depending on size and charge). A single droplet is moved from the upper to the lower compartment by setting the upper DC balancing voltage to zero for approximately 10 – 50 ms (Figure 1b). Once trapped in the lower compartment a droplet can be sized as described below, and ejection from the trap is facilitated by removing the balancing voltage in the lower compartment. A grounded exit plate terminates fields at the base of the QET and facilitates reliable single droplet ejection.

The QET is enclosed in an environmentally controlled chamber where humidity is controlled by a nitrogen or zero air flow of up to 500 $cm^3\,min^{-1}$ (STP), split into a dry flow and a wet flow that passes through a water bubbler. The magnitude of the wet and dry flow are controlled by mass flow controllers (MKS instruments), and their relative magnitude determines the relative humidity in the trap, which was monitored with an RH probe (Honeywell International Inc., HIH-4602C, ±3.5% accuracy) at the QET inlet. Experiments were performed at high humidity (∼75-90% RH). The gas flow provides a downward force that further facilitates droplet ejection from the QET to the ionization region.

Droplet sizing

Trapped droplets are illuminated axially with a 532 nm laser (ThorLabs, CPS532), introduced into the top of the QET and focused toward the lower sizing compartment (Figure 1a). For both droplet positioning in the trap and droplet sizing, scattered light is collected on two CCD cameras (ThorLabs, DCC1645C) [40,42]. A levitated droplet is maintained within the trap's lower compartment using a feedback loop in a custom LabView software that controls both the DC balancing voltage and AC frequency in response to changes in droplet size and position above the balancing electrode. Droplets are sized using interference fringes in the Mie scattering pattern collected at 90°, with the method described by Davies [41]. Briefly, angular peak positions (i.e., distinct maxima in the angular scattering pattern) are iteratively compared with a library of simulated peak positions, generated with Mie theory over a range of size and refractive index. For a fixed refractive index, estimated from droplet composi-

tion and water content, a measure of the difference between reference and recorded peak positions is minimized to extract the best fitting droplet size[41]. This method can provide radius measurements with an accuracy of up to ±60 nm; however, due to uncertainties in the angular width of scattered light collected in our experiment we estimate a larger uncertainty of ±0.5 µm in diameter. When direct measurements of droplet size are not available, the dry droplet size and mass of solute dispensed can be estimated based on the initial size of the dispensed droplet and the initial solution concentration. The initial droplet diameter from the 30 µm dispenser is on the order of 50 µm in diameter[37,42].

Single Droplet Ambient Ionization Mass Spectrometry

All measurements were carried out with a QExactive Orbitrap Mass Spectrometer (ThermoFisher Scientific). The instrument was operated in negative ion mode, with a typical scan range of m/z ∼ 50 – 200, a resolution of 17500 and a maximum inject time of 50 ms, resulting in a scan rate of 8 – 9 Hz. The QET was positioned above the mass spectrometer inlet and was coupled to a home-built ambient pressure ionization source by a grounded, 1/4" stainless steel exit tube. Two complementary ionization sources are used in these experiments: paper spray ionization and thermal desorption coupled to helium glow discharge ionization (Figure 1b). The basic principles of these ionization techniques have been described elsewhere[43–46], and below we describe the design of these ionization sources for single droplet detection.

Paper spray ionization

Two types of paper substrate were used for paper spray (PS) ionization in this work: Whatman grade 3MM chromatography paper (0.34 mm thickness) and Whatman grade SG81 silica-coated chromatography paper (0.27 mm thickness), which has been shown previously to improve sensitivity of PS-MS analysis for some compounds[47]. Papers were cut into triangular substrates with rounded lower corners using a universal laser cutter, to create substrates

with a base of 8 mm and height of 10 mm, leading to a spray tip angle of ∼45°. Other geometries and substrates were tested; however, a rigorous evaluation is not presented here as other work has characterized the impact of spray tip angle and substrates on PS-MS performance[48–51]. Paper substrates were mounted in a stainless steel alligator clip and a voltage of −3 kV to −5 kV was applied to the solvent-soaked substrate. Solvent (either HPLC grade methanol, or a methanol-chloroform mixture) was continuously supplied to the underside of the substrate with a PEEK delivery tube connected to a syringe pump operating at 20 – 30 µL min^{-1}.

Thermal desorption glow discharge ionization

A home-built helium glow discharge (GD) ionization source, similar to the home-built DART source described by Upton et al.[52], was coupled to a temperature controlled vaporization platform for single droplet detection (Figure 1b). The GD source was constructed from 1/16" tungsten electrodes housed in 3/8" outer diameter glass tubing, with 1/4" outer diameter glass tubing for the gas connection line. The GD source was run with 0.5 L min^{-1} (STP) helium flow, controlled with a mass flow controller (MKS Instruments). The needle electrode was tapered to a point and operated at 3 kV with a current of ∼2.7 mA limited by a 1 MΩ (10 W) resistor, and a discharge gap of ∼ 2.5 mm from the flat-ended ground electrode. This configuration corresponds to the corona-to-glow discharge (DART-like) regime described by Shelley et al.[53]. Outflow from the GD source, containing helium ions and metastable atoms, entered a 1/4" through-way in a heated stainless steel vaporizing block held at ground. The vaporizer temperature was controlled with a cartridge heater (1" x 1/4", 100 W) connected to a temperature controller (Omega Engineering, CN9300). The MS inlet was positioned ∼2 mm within the 1/4" outlet of the vaporizer. The QET outlet was connected to a 1/4" port on the vaporizer that was orthogonally offset ∼5 mm from the helium stream. Ejected droplets impact the heated substrate in the QET gas flow and the resulting gas phase molecules intersect with the GD outflow in the ionization region to form

ions sampled by the MS. The total flow directed toward the MS inlet was $1\,\mathrm{L\,min^{-1}}$ (STP), with an absolute humidity a factor of two lower than that in the QET due to dilution by dry helium.

Data analysis

Raw mass spectra were initially analyzed using the python based pymsfilereader (available at: github.com/frallain/pymsfilereader, using python 3.7.3), and Thermo Xcalibur. Time series of relevant exact masses were extracted for further analysis. Single droplet events were defined as signals a specified number of standard deviations (generally >5) above a running mean baseline. The detected signals were integrated to provide the peak area corresponding to a single droplet at a particular exact mass-to-charge ratio, referred to as $\mathrm{I_X}$, where X is the droplet component of interest. The duration of droplet signals for a specific droplet component were determined by the time window for droplet signal integration. Droplet evaporation was modeled assuming constant isothermal evaporation from a sphere, as in Birdsall et al.[38]. The AIOMFAC model (aiomfac.caltech.edu) was used to calculate droplet water content[54]. Data analysis and evaporation model code is available at github.com/willismd.

Droplet Heterogeneous Reaction Kinetics

Ozone was generated by passing a small flow of oxygen, $20 - 100\,\mathrm{cm^3\,min^{-1}}$ (STP), through a glow discharge ozone generator, and diluting the resulting flow with $2 - 4\,\mathrm{L\,min^{-1}}$ (STP) of nitrogen. The resulting flow ($100 - 700\,\mathrm{ppm\ O_3}$) was sampled by an ozone monitor (2B Technologies, model 202M) and a small portion, $\sim 35 - 60\,\mathrm{cm^3\,min^{-1}}$ (at STP), was diverted through a rotameter and mixed with the wet gas flow entering the QET.

The general experimental sequence is outlined in Figure 1b. Following trapping of a droplet population, sizing and MS detection of unreacted single droplets, the dry component of the QET flow is replaced by an equal mass flow containing ozone, such that the relative humidity in the trap is maintained within 1 – 2%. Trapped droplets are exposed to ozone

for a period of time, during which the outflow of the QET is sent to exhaust, and the size of a single droplet can be monitored in the sizing compartment. After an exposure time has elapsed ozone generation is switched off and a series of single droplets ($\geq$8) are individually ejected for MS detection, so that ozone is not present in the ionization region during droplet detection. By repeating this process over the course of minutes to hours, we follow the kinetics of the reaction between droplet components and ozone in time.

Results and Discussion

Single Droplet Paper Spray Ionization Mass Spectrometry

Detection of single aqueous droplets

Negative mode PS-MS detects organic acids in aqueous droplets with high signal-to-noise ratios and negligible fragmentation of deprotonated molecular ions. Individual droplets containing 0.5 ng maleic and 3.1 ng malonic acid, with a volume of 6 pL at 85% humidity, were easily detected above background by PS-MS with signal-to-noise ratios >100 (Figure 2a). After ejection of a single aqueous droplet from the QET, signals for $[M-H]^-$ ions for both acids ($C_3H_3O_4^-$ at m/z 103.00 and $C_4H_3O_4^-$ at m/z 115.00) quickly increase and decay away over a duration of ~9 seconds (Figure 2a). A characteristic peak in the background PS-MS mass spectrum is HSO_4^- (m/z 96.96), which has been observed in other implementations of PS-MS[37] (Figure 2b). The presence of droplet components in a single droplet mass spectrum is clearly detected above background (Figure 2c). For a 30 µL min^{-1} solvent flow and a droplet event that lasts 9 seconds (Figure 2a), we estimate a mean malonic and maleic acid concentrations of 0.7 ng µL^{-1} and 0.1 ng µL^{-1}, respectively, in the spraying solution.

Several factors influence the reproducibility of single droplet detection by PS-MS, two of which are universal to all ionization techniques applied to single droplet measurements. First, the MS sampling rate must be sufficiently high to provide a well-defined single droplet

signal. For sampling rates >1 Hz and droplet events lasting several seconds this requirement should not impede reproducibility. Second, variations in the droplet size produced by the dispensers can be on the order of the few percent around the mean diameter, which could produce non-negligible changes in the mass of solute dispensed. Our size measurements suggest this variability can be on the order of ±2.5% in diameter, which corresponds to variability in droplet mass of ∼10%. We discuss factors specific to PS-MS droplet detection next.

Impact of solvent and spray tip position on single droplet detection

PS-MS specific considerations for reproducibility are spray stability and droplet deposition location[37]. Negative ion mode PS-MS has intrinsic challenges related to the high current involved, and addition of $CHCl_3$ to the spray solvent has been shown to mitigate the formation of corona discharges from fibres at the spray tip[44,55]. Use of ≥20% $CHCl_3$ (v/v) in our spray solvent significantly improved spray stability and both the efficiency and reproducibility of single droplet detection (Figure S1). The spray tip was mounted ∼1 cm from the MS inlet, and the grounded QET outlet was positioned ∼1 cm above the spray substrate (Figure S1). While positioning the spray tip closer to the MS inlet would provide enhanced signal intensity[56], the geometry of our apparatus is constrained by the QET size and shape. With negative ion mode PS-MS, positively charged single droplets are ejected from the QET and are attracted toward the spray tip. The deposition location of droplets on the paper substrate impacts both the single droplet event timescale and reproducibility, as described for free-falling neutral droplets by Kaur Kohli and Davies[37]. We observe good reproducibility in droplet signals with the spray tip positioned in line with the edge of the QET outlet, such that droplets likely land slightly behind the spray tip[37]. We discuss the precision and accuracy of single droplet PS-MS more quantitatively below.

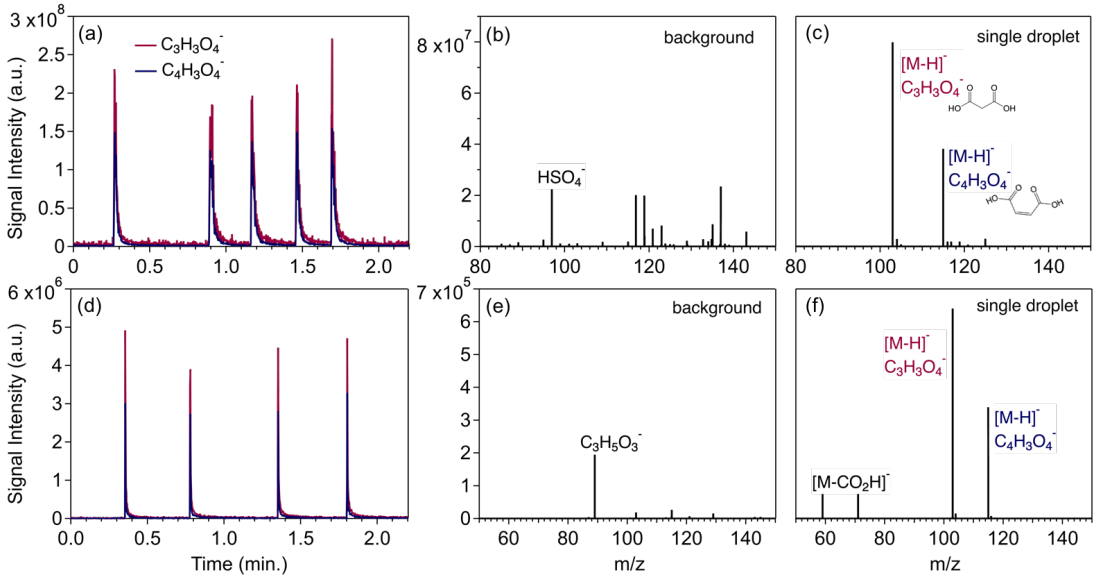

Figure 2: (a) Examples of negative mode PS-MS single droplet events from deprotonated molecular ions of malonic ($C_3H_3O_4^-$, m/z 103.00) and maleic acid ($C_4H_3O_4^-$, m/z 115.00) for droplets containing 0.5 ng maleic and 3.1 ng malonic acid (estimated assuming 50 µm initial droplet size), corresponding to an equivalent dry diameter 16.2 µm. (b) PS-MS background mass spectrum, showing the prevalent peak for bisulfate (HSO_4^-, m/z 96.96). (c) Background subtracted single droplet PS mass spectrum, shown on the same y-scale as (b), and corresponding to the mean mass spectrum over one peak in (a). (d) – (f) As in (a) – (c), but for TDGD-MS. The dominant peak in the negative mode TDGD-MS background spectrum (at 120 °C), in (e), is deprotonated lactic acid ($C_3H_5O_3^-$, m/z 89.02). Some decarboxylation of malonic and maleic acid is evident in TDGD-MS single droplet spectra (f).

Single Droplet Thermal Desorption, Glow Discharge Ionization Mass Spectrometry

Detection of single aqueous droplets

Thermal desorption coupled to glow discharge ionization MS (TDGD-MS) in negative ion mode detects organic acids in aqueous droplets with comparable sensitivity to PS-MS, despite lower absolute signal intensities. TDGD-MS signals arising from individual picoliter droplets containing 0.5 ng maleic and 3.1 ng malonic acid are shown in Figure 2d, with signal-to-noise ratios of ∼500. Ejection of single droplets from the QET gives rise to sharp signals for $[M-H]^-$ ions corresponding to these organic acids, which rapidly decrease over about 6 seconds (depending on vaporization temperature, discussed below). The background mass spectrum, taken during a period just before droplet detection appears significantly cleaner than for PS-MS, with the dominant peak between m/z 50 – 150 being the singly deprotonated molecular ion of lactic acid ($C_3H_5O_3^-$, m/z 89.02) (Figure 2e). Lactic acid is likely desorbing from surfaces within the vaporizer and QET, and is present at relatively constant signal intensity within the GD-MS background at constant vaporizer temperature. Similarly to PS-MS, the presence of droplet components are clearly apparent above the background; however, a fraction of the $[M-H]^-$ ions undergo loss of CO_2 to form fragments at m/z 59.01 ($C_2H_3O_2^-$) and m/z 71.01 ($C_3H_3O_2^-$) for maleic and malonic acid, respectively (Figure 2f). For a QET flow of 500 $cm^3\,min^{-1}$ and a droplet event lasting ∼6 seconds (Figure 2d), we estimate mean gas phase malonic and maleic acid concentrations of 78 $pg\,cm^{-3}$ and 12 $pg\,cm^{-3}$ (at STP), respectively. Multiple factors influence both the sensitivity and reproducibility of TDGD-MS droplet detection, and are discussed below.

Impact of humidity on ionization of organic acids

The amount of water vapour in the region of ion formation significantly impacts the efficiency of $[M-H]^-$ formation from organic acids by TDGD-MS. We use lactic acid in the TDGD-

MS background as a qualitative indictor of water vapour's impact on $[M-H]^-$ formation from organic acids. As the amount of water vapour increases from near zero (i.e., a dry QET flow) to ∼0.02 atm (i.e., ∼95% RH QET flow at 25 °C), lactic acid $[M-H]^-$ ion signal intensity significantly increases (Figure 3a). Reaching higher water vapour concentrations in our current iteration of TDGD-MS is not possible as the flow of dry helium is fixed and the maximum practical flow through the QET is 500 $cm^3\,min^{-1}$, leading to a maximum relative humidity in ionization region on the order of 48% RH at 25 °C. However, higher humidities may not result in further enhanced $[M-H]^-$ formation, as we begin to observe a levelling in lactic acid signal intensity at the highest humidities available in our set up (Figure 3a).

Previous studies demonstrate an effect of humidity on low temperature plasma ionization sources[57–59]. Overall, previous work shows that water concentration can change relative reagent ion abundances, analyte signal intensities and extent of fragmentation. The impact of humidity on sensitivity is a well known phenomenon in chemical ionization MS, where sensitivity can depend strongly on sample humidity[60–63]. The ultimate impact of humidity will depend upon the reagent ion and the relevant ionizations mechanisms.

Our observations show evidence for OH^- as a dominant reagent ion for deprotonation of organic acids by helium glow discharge ionization. In our experiment, where the ionization region is closed to ambient air, the presence of water has a much larger influence on $[M-H]^-$ formation from lactic acid than the presence of oxygen (Figure 3b). We are unable to measure mass-to-charge ratios below 50 with the QExactive, so we infer the presence of a gas phase base associated with the presence of water vapour. OH^- is a very strong gas phase base that reacts rapidly and effectively to form $[M-H]^-$ ions from species with even mildly acidic protons[64,65], and has been used as a reagent ion for chemical ionization MS[66,67]. Cody et al.[45] suggest that $O_2^{\bullet-}$ is a dominant reagent ion in negative mode DART ionization. However, direct measurements of DART reagent ions have demonstrated the presence of other basic anions such as OH^-[65], which forms in the reaction of water with excited helium atoms[45]. In ambient air a significant fraction of OH^- is present as HCO_3^-, its reaction product with

CO_2, when acids are not present[45,65]. OH^- has a high hydration energy and clustering with water vapour tends to decrease the efficiency of ion-molecule reactions[64], suggesting that at elevated humidities $[M-H]^-$ formation by OH^- could become less favourable and care must be taken to optimize conditions for different analytes.

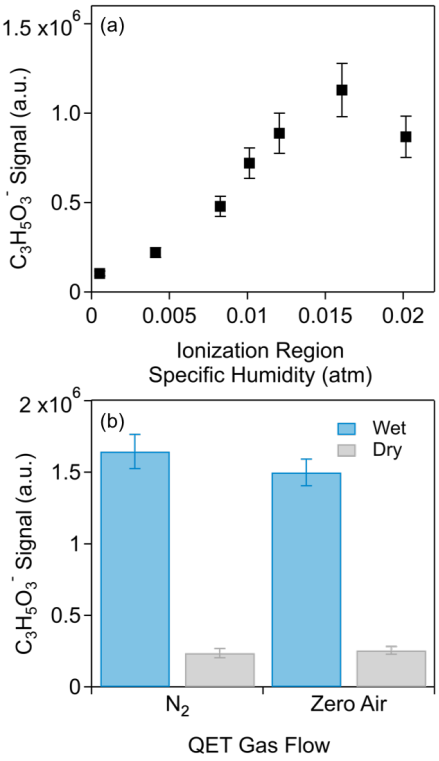

Figure 3: (a) Impact of humidity on the glow discharge ionization signal intensity for lactic acid $[M-H]^-$ ions ($C_3H_5O_3^-$, m/z 89.02), with constant QET and glow discharge helium flows meeting in the ionization region. (b) The presence of water vapour in the GD-MS ionization region has a larger impact on $C_3H_5O_3^-$ signals than the presence of oxygen. Wet and dry QET gas flows correspond to ~0 atm H_2O and 0.02 atm H_2O in the ionization region. Error bars correspond to the standard deviation in signal intensities over ~10 minutes at 8 Hz.

Impact of vaporization temperature on single droplet detection

Vaporization temperature can impact both the precision and accuracy of TDGD-MS single droplet detection. At a constant droplet size, changes in vaporization temperature drive changes in analyte evaporation rates, which results in two important effects. First, the timescale of single droplet detection events dictate how well a droplet signal is defined at a

fixed MS sampling rate (Figure 4a). At higher temperatures I_X decreases, and variability in I_X can increase because fewer data points define the droplet signal (Figure 4b). Second, higher gas phase concentrations of analyte in the ionization region increase the potential for significant ion suppression. For the mass of maleic and malonic acid shown here, this effect becomes evident at temperatures above ∼135 °C, where $I_{malonic}$ decreases more steeply with temperature than I_{maleic} and the corresponding ratio increases (Figure 4b,c). Analogous ionization suppression by a gas phase matrix has been previously observed with plasma-based ambient ionization MS sources[68]. Though we cannot directly detect the reagent ion in our instrument, the lactic acid background can provide qualitative indication of ion suppression at high evaporation rates. In cases of high evaporation rates (i.e., high temperature and high solute mass), the signal for lactic acid can be suppressed to zero, indicating limitations for quantitative ability (Figure S2a). These issues are avoided by selecting appropriate droplet vaporization temperatures and small solute masses (Figure S2b, Figure 4 shaded region). The optimal range of droplet vaporization temperatures is related to analyte volatility, and this effect is discussed next.

Impact of volatility on single droplet detection

At constant droplet size and vaporization temperature, the volatility of droplet components drives the timescale for single droplet detection. We demonstrate this effect for droplets containing nanogram quantities of multifunctional organic compounds of varying vapour pressure: maleic, succinic, tartartic and citric acids. We observe sequential evaporation of the four acids (Figure 5a), which suggests that the droplets remain in a liquid state at evaporation even though particle-phase water has likely completely evaporated during transit to the vaporizer[69]. We detect all acids as $[M-H]^-$ ions, with some fragmentation through loss of CO_2 for maleic, succinic acids, and both CO_2 and H_2O from citric acid (Figure 5b). For multiple monodisperse droplets, we observe consistent absolute integrated signal intensities (RSD ∼10%) for each compound and correspondingly consistent measured sizes (Figure 5c).

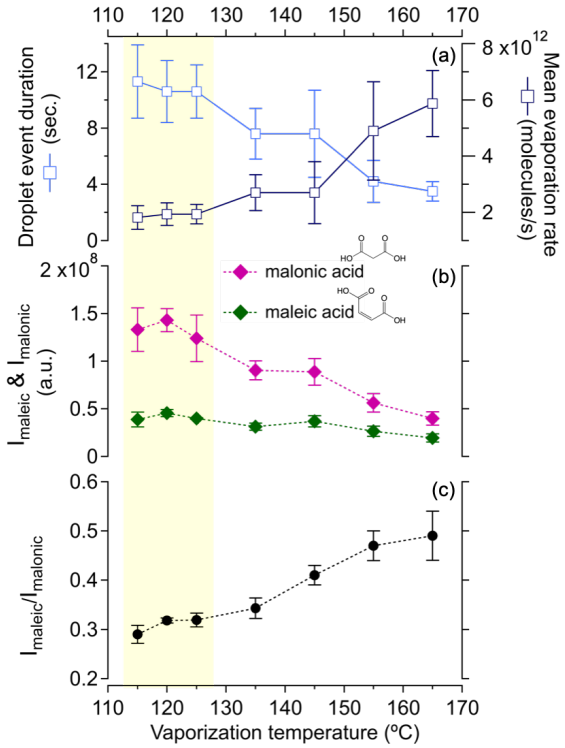

Figure 4: Impact of droplet vaporization temperature on (a) the duration of droplet signals in time (left axis) and estimated mean evaporation rates (right axis) for droplets containing 0.5 ng maleic and 3.1 ng malonic acid (dry diameter ∼16.2 µm), (b) absolute integrated droplet signal intensities, and (c) the ratio of integrated droplet signals. The shaded yellow region represents ideal sampling conditions for maleic and malonic acid droplets in this size range.

The timescale for evaporation of each droplet component is related to its vapour pressure at the vaporization temperature (Figure 5d), though we emphasize that droplet size also has a significant impact impact on the evaporation rate. The longer evaporation timescale and correspondingly lower evaporation rates for less volatile compounds (i.e., tartaric and citric acids) reduces the potential for the significant ionization suppression discussed for the more volatile acids (Figure 4, Figure S2b). As a consequence, simultaneous detection of droplet components with significantly different volatilities, such organics mixed with inorganic salts, represents a compromise between the high temperatures required for detection of very low volatility compounds and the impact of high organic evaporation rates on TDGD-MS precision and accuracy.

Accuracy and Precision of Single Droplet Measurements

Accurate and precise measurements of single droplet composition are possible with both PS-MS and TDGD-MS. Day-to-day, and for PS-MS paper-to-paper, differences exist in the absolute I_X for a series of individual droplets with nominally identical composition (Figure 6a&d). This difference in mean signals can be accounted for in two ways. First, signals in the background mass spectrum can be used to account for variability in GD ionization efficiency or PS spray characteristics[37]. By normalizing TDGS-MS signals to lactic acid and PS-MS signals to bisulfate, the mean $I_X/I_{background}$ is brought into agreement for both ion sources (Figure 6b&e). While this approach demonstrates the quantitative ability of these techniques, increased variability from the background ions is introduced into the ratio, and can be a large as $\pm 50\%$ for PS-MS. Droplet-to-droplet reproducibility in absolute I_X within a data set is generally better for TDGD-MS (RSD $<25\%$, Figure 6d & Figure 4) than for PS-MS (RSD $\sim 25\%$, Figure 6a). Second, a droplet internal standard can be used to improve both the precision and accuracy of single droplet measurements. A droplet internal standard accounts for multiple ion source related factors that affect droplet-to-droplet reproducibility, including PS stability and variation in droplet deposition location, GD ion transmission

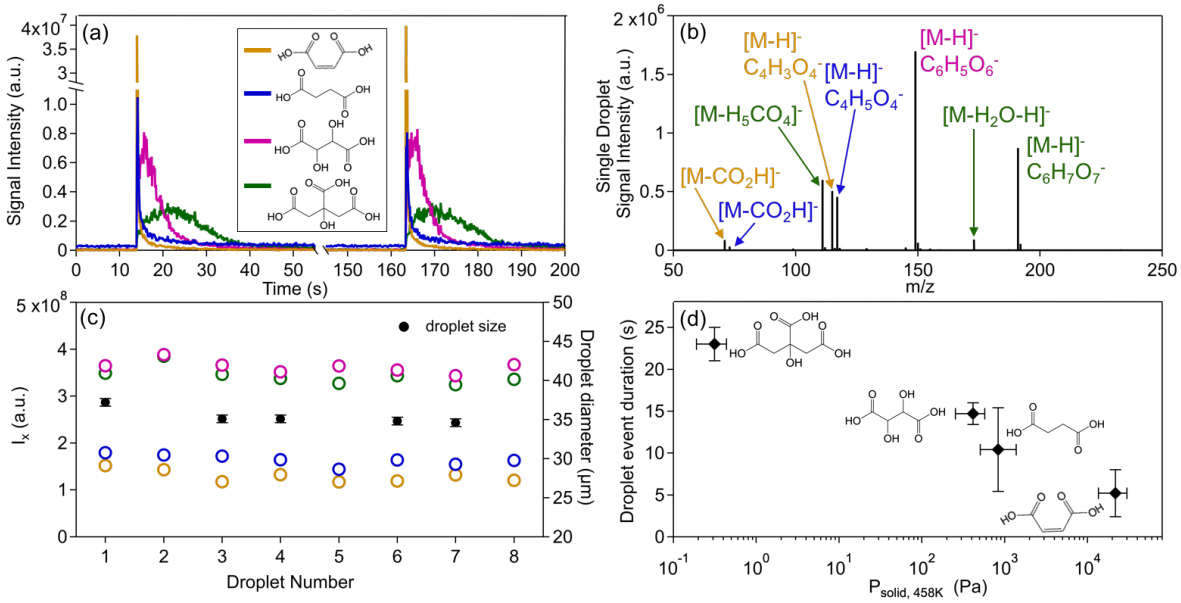

Figure 5: Impact of vapour pressure on single droplet detection by TDGD-MS. (a) Example single droplet events for four component droplets containing 3.4 ng maleic acid, 3.2 ng succinic acid, 6.5 ng tartaric acid, and 7.2 ng citric acid (dry diameter ∼28 µm), evaporated at 160 °C. (b) Mean single droplet mass spectrum, showing deprotonated molecular ions and corresponding fragments for each acid. (c) Demonstration of the reproducibility of absolute integrated droplet signals (I_X, left axis) for each droplet component, and the corresponding measured droplet diameter when sizes were available (right axis). Colours correspond to the legend in (a). (d) Relationship between the vapour pressure of each droplet component at 160 °C, and the mean droplet event duration from TDGD-MS measurements. X-axis error bars correspond to the range in recommended vapour pressures reported in Bilde et al. [70] and Dennis-Smither et al. [21], and y-axis error bars correspond to the standard deviation in droplet event duration across 13 droplets.

and variations in vaporization temperature. Further, a droplet internal standard corrects for variations in droplet size. The ratio of I_{maleic} to $I_{malonic}$ in the same droplets provides both precisions consistently on the order of $\pm 5\%$ or less, and improved agreement between measurements made on multiple days and with different PS-MS substrates (Figure 6c&f).

With a droplet internal standard, both PS-MS and TDGD-MS respond linearly and reproducibly to a range of droplet solute concentrations. We demonstrate the linearity and reproducibility of both techniques with droplets containing 0.2 ng to 1.2 ng maleic acid and a constant 3.1 ng malonic acid, resulting in equivalent dry diameters of 15.7 µm to 17.1 µm (∼5–7 pL at 85% humidity). Individual points in Figure 7 correspond to mean integrated droplet signals for different populations of droplets on different days, and detected with different papers for PS-MS, while error bars on each point correspond to the standard deviation from ≥8 single droplets. $I_{maleic}/I_{malonic}$ versus the molar ratio of these two droplet components ($n_{maleic}/n_{malonic}$) gives a slope corresponding to the relative ionization efficiency of maleic to malonic acid (Figure 7). Relative ionization efficiencies demonstrate that both PS-MS and TDGD-MS are more sensitive to maleic than malonic acid, consistent with resonance stabilization of the singly deprotonated anion of maleic acid and a pKa ∼1 pH unit lower than malonic acid. Maleic acid signal-to-noise ratios for the lowest concentration in Figure 7 are ∼500 for both PS-MS and TDGD-MS, demonstrating a detection limit (S/N = 10) on the order of 5 pg (1.8 µm dry diameter). Signal-to-noise ratios for malonic acid differed more significantly between the two ionization sources (∼100 and ∼450, respectively), giving detection limits on the order of 300 pg (7 µm dry diameter) and 65 pg (4.3 µm dry diameter), for PS-MS and TDGD-MS, respectively.

Reaction Kinetics from Single Droplet Mass Spectrometry

We demonstrate application of our QET coupled to single droplet MS to following the reactive loss of maleic acid with gas phase O_3, and report a reactive uptake coefficient comparable to previous measurements. We follow the reaction by measuring the relative composition

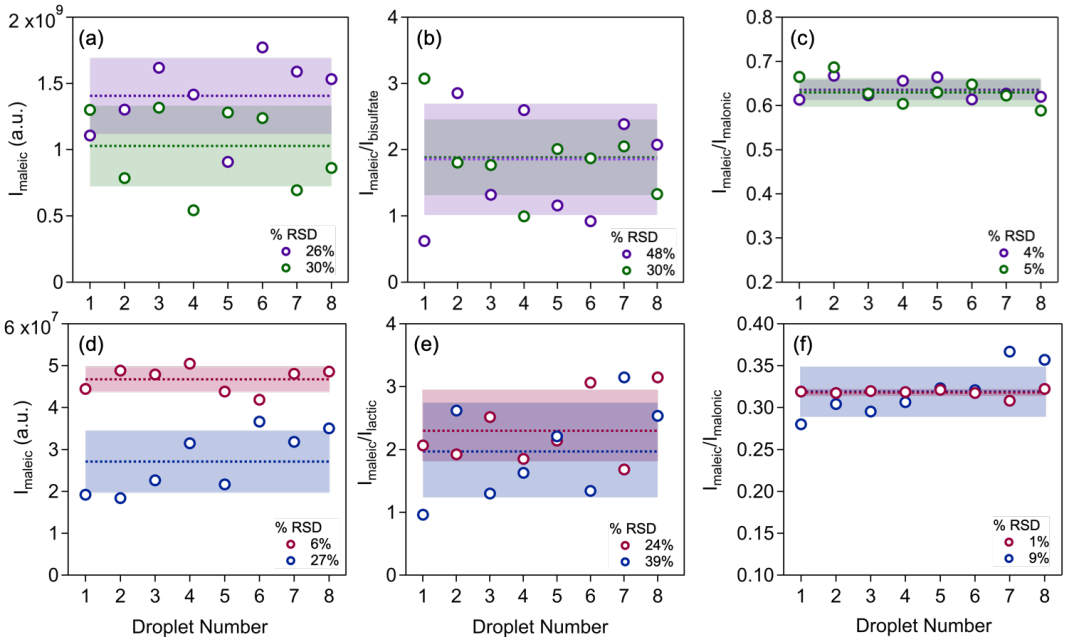

Figure 6: Demonstration of single droplet MS precision and accuracy across multiple measurements for PS-MS (top) and TDGD-MS (bottom). (a) & (d) Absolute I_{maleic} across 2 sets of 8 droplets events for PS-MS and TDGD-MS, respectively. Colours represent different measurement days, and for PS-MS different paper substrates. (b) & (e) I_{maleic} normalized to characteristic background signals in PS-MS ($I_{bisulfate}$) and TDGD-MS (I_{lactic}). (c) & (f) I_{maleic} normalized to $I_{malonic}$ as a droplet internal standard. Dashed lines represent the mean, and shading represents ± one standard deviation.

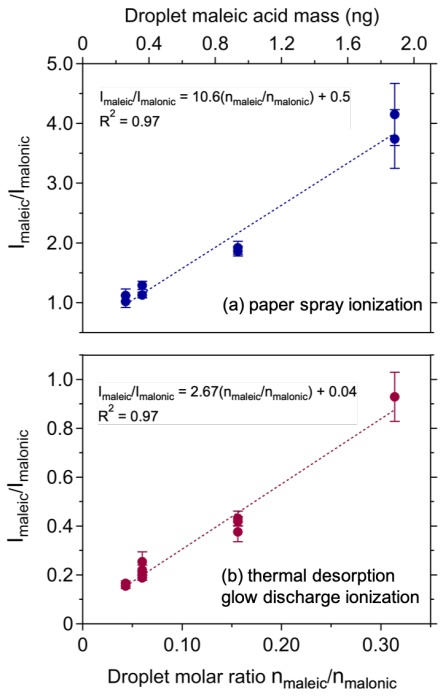

Figure 7: Both PS-MS (a) and TDGD-MS (b) provide a linear response to increasing maleic acid mole fraction in droplets, with malonic acid as a droplet internal standard. The slope of $I_{maleic}/I_{malonic}$ versus the molar ratio of maleic to malonic acid gives the relative ionization efficiency. All droplets contain approximately 3.1 ng malonic acid, and 0.2 ng to 1.2 ng maleic acid (top axis), corresponding to dry diameters of 15.7 µm to 17.1 µm. Each data point corresponds to single droplets measured on different days, and different paper substrates for PS-MS. Error bars reflect the standard deviation in $\geq$8 single droplet events.

of single droplets at discrete time points using TDGD-MS, where each point in Figure 8 corresponds to mean I_{maleic} from $\geq$8 single droplets. We follow droplet reaction kinetics with TDGD-MS here since our previous work has demonstrated reaction monitoring with PS-MS[40], and as described above TDGD-MS provides better droplet-to-droplet reproducibility in absolute I_X. Over the timescale of our reaction, both our measurements and a kinetic model of droplet evaporation indicate that evaporative loss is negligible compared to reaction with 50 ppm O_3 (Figure 8). Formulating an expression for the uptake coefficient assuming reaction takes place at the droplet surface, and fitting the observations to an exponential decay[71], yields an effective uptake coefficient (γ_{eff}) of 4.4($\pm$0.5)x10^{-5} (assuming an initial droplet size of 50 µm, that equilibrates to 84% humidity in the QET). Other investigations of O_3 reacting with maleic acid in aqueous particles have assumed the reaction occurs in the droplet bulk and is limited by ozone diffusion. For example, Dennis-Smither et al.[21] follow the reaction in an electrodynamic balance with Raman spectroscopy and arrive at γ_{eff} of (2.7–9.9)x10^{-6}, at humidities above 50% and 38 ppm to 67 ppm O_3. However, noise in their Raman signals prevented clear discrimination between exponential and quadratic fits to their observations[21]. If we apply an uptake model assuming reaction in the bulk, we arrive at a γ_{eff} of 8.7($\pm$2.0)x10^{-6} (Figure S3). Earlier reports of γ_{eff} are on the same order, where values of (0.7–7.6)x10^{-6} and (0.3–1.8)x10^{-5} were obtained assuming near-surface[72] and bulk[18] reaction kinetics, respectively, for aqueous particles at humidities above 80%. While the lack of direct size measurements associated with our kinetic data introduces uncertainty into our determination of γ_{eff}, our observations agree with previous measurements within the range of values reported and suggest the QET-MS can be successfully applied to studying reactive transformations in single droplets.

Single droplet mass spectra (Figure S4) at various extents of oxidation suggest that any products formed either volatilize from the droplets (i.e., glyoxylic acid[73]), are below detection limits, or fragment significantly during thermal vaporization. Product detection can be optimized by measuring multiple droplets concurrently to increase signal intensities,

varying vaporization temperature, and applying PS-MS for detection of thermally unstable products.

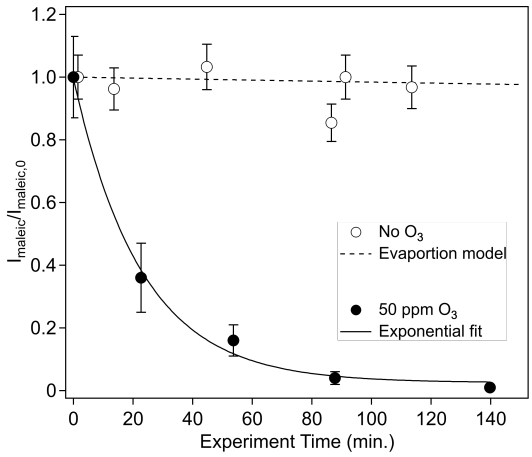

Figure 8: Demonstration of reaction kinetics of O_3 and maleic acid in aqueous droplets (84(±3)% RH) followed with TDGD-MS. Open circles correspond to $I_{maleic}/I_{maleic,0}$ measured in the absence of O_3, and the dashed lines shows results from a model of maleic acid evaporation from the droplet. Filled circles correspond to $I_{maleic}/I_{maleic,0}$ measured in the presence of 50 ppm O_3. The black solid line is a single exponential fit, providing an effective uptake coefficient (γ_{eff}) of 4.4(±0.3)x10^{-5}. Error bars represent the standard deviation of ≥8 single droplet events.

Conclusions

We present a new approach for studying the chemistry of droplet populations by coupling levitated droplets in a multi-compartment electrodynamic trap to single droplet mass spectrometry. Trapping a population of monodisperse droplets confers advantages for reproducibility and the experimental timescales needed to obtain statistically meaningful results across multiple droplets. Using this technique, we show a direct comparison between ambient ionization sources for detection of single aqueous droplets. Both PS-MS and TDGD-MS respond linearly and reproducibly to low nanogram to picogram quantities of oxygenated organic molecules in picoliter droplets, with detection limits on the order of 5 pg for maleic acid. These two droplet detection techniques are complementary, and provide distinct advantages. While TDGD-MS can detect organic compounds in mixtures with salts that are

not amenable to PS-MS, TDGD-MS has limitations for detecting fragile organic molecules that fragment upon vaporization but remain intact in PS-MS. Complementary soft ionization techniques, coupled with non-destructive optical probes of microphysical properties in the QET, will provide valuable insight into heterogeneous and multiphase reactions over a wide range of timescales and oxidant concentrations.

Acknowledgement

The authors thank Dr James Davies and Ravleen Kaur Kohli (UC Riverside) for helpful discussions, Dr Lance Lee (Stanford Research Systems) for the original design of the quadrupole trap, and Bruce Rude (LBNL) for technical support. MDW acknowledges support from a Natural Sciences and Engineering Research Council of Canada (NSERC) postdoctoral fellowship. This work was supported by the Condensed Phase and Interfacial Molecular Science Program, in the Chemical Sciences Geosciences and Biosciences Division of the Office of Basic Energy Sciences of the U.S. Department of Energy under Contract No. DE-AC02-05CH11231.

Supporting Information Available

The following files are available free of charge.

- Supporting Information. Figure S1: PS-MS solvent composition. Figure S2: Ion suppression in TDGD-MS. Figure S3: Kinetic data.

This material is available free of charge via the Internet at `http://pubs.acs.org/`.

References

(1) Krieger, U. K.; Marcolli, C.; Reid, J. P. Exploring the complexity of aerosol particle properties and processes using single particle techniques. *Chem Soc Rev* **2012**, *41*,

6631–6662.

(2) Poschl, U.; Shiraiwa, M. Multiphase Chemistry at the Atmosphere-Biosphere Interface Influencing Climate and Public Health in the Anthropocene. *Chem Rev* **2015**, *115*, 4440–4475.

(3) Bzdek, B. R.; Reid, J. P. Perspective: Aerosol microphysics: From molecules to the chemical physics of aerosols. *J Chem Phys* **2017**, *147*, 220901.

(4) Soonsin, V.; Zardini, A. A.; Marcolli, C.; Zuend, A.; Krieger, U. K. The vapor pressures and activities of dicarboxylic acids reconsidered: the impact of the physical state of the aerosol. *Atmos Chem Phys* **2010**, *10*, 11753–11767.

(5) Davies, J. F.; Haddrell, A. E.; Rickards, A. M.; Reid, J. P. Simultaneous analysis of the equilibrium hygroscopicity and water transport kinetics of liquid aerosol. *Anal Chem* **2013**, *85*, 5819–26.

(6) Rovelli, G.; Miles, R. E.; Reid, J. P.; Clegg, S. L. Accurate Measurements of Aerosol Hygroscopic Growth over a Wide Range in Relative Humidity. *J Phys Chem A* **2016**, *120*, 4376–88.

(7) Boyer, H. C.; Gorkowski, K.; Sullivan, R. C. In Situ pH Measurements of Individual Levitated Microdroplets Using Aerosol Optical Tweezers. *Anal Chem* **2020**, *92*, 1089–1096.

(8) Cohen, L.; Quant, M. I.; Donaldson, D. J. Real-Time Measurements of pH Changes in Single, Acoustically Levitated Droplets Due to Atmospheric Multiphase Chemistry. *ACS Earth and Space Chemistry* **2020**, *4*, 854–861.

(9) Bzdek, B. R.; Power, R. M.; Simpson, S. H.; Reid, J. P.; Royall, C. P. Precise, contactless measurements of the surface tension of picolitre aerosol droplets. *Chem Sci* **2016**, *7*, 274–285.

(10) Rovelli, G.; Song, Y. C.; Maclean, A. M.; Topping, D. O.; Bertram, A. K.; Reid, J. P. Comparison of Approaches for Measuring and Predicting the Viscosity of Ternary Component Aerosol Particles. *Anal Chem* **2019**, *91*, 5074–5082.

(11) Richards, D. S.; Trobaugh, K. L.; Hajek-Herrera, J.; Davis, R. D. Dual-Balance Electrodynamic Trap as a Microanalytical Tool for Identifying Gel Transitions and Viscous Properties of Levitated Aerosol Particles. *Anal Chem* **2020**, *92*, 3086–3094.

(12) Gorkowski, K.; Beydoun, H.; Aboff, M.; Walker, J. S.; Reid, J. P.; Sullivan, R. C. Advanced aerosol optical tweezers chamber design to facilitate phase-separation and equilibration timescale experiments on complex droplets. *Aerosol Sci Technol* **2016**, *50*, 1327–1341.

(13) Haddrell, A.; Rovelli, G.; Lewis, D.; Church, T.; Reid, J. Identifying time-dependent changes in the morphology of an individual aerosol particle from its light scattering pattern. *Aerosol Sci Technol* **2019**, *53*, 1334–1351.

(14) Price, C. L.; Bain, A.; Wallace, B. J.; Preston, T. C.; Davies, J. F. Simultaneous Retrieval of the Size and Refractive Index of Suspended Droplets in a Linear Quadrupole Electrodynamic Balance. *J Phys Chem A* **2020**, *124*, 1811–1820.

(15) Dennis-Smither, B. J.; Hanford, K. L.; Kwamena, N. O.; Miles, R. E.; Reid, J. P. Phase, morphology, and hygroscopicity of mixed oleic acid/sodium chloride/water aerosol particles before and after ozonolysis. *J Phys Chem A* **2012**, *116*, 6159–68.

(16) Westphall, M. S.; Jorabchi, K.; Smith, L. M. Mass spectrometry of acoustically levitated droplets. *Anal Chem* **2008**, *80*, 5847–5853.

(17) Lee, A. K. Y.; Chan, C. K. Single particle Raman spectroscopy for investigating atmospheric heterogeneous reactions of organic aerosols. *Atmos Env* **2007**, *41*, 4611–4621.

(18) King, M. D.; Thompson, K. C.; Ward, A. D.; Pfrang, C.; Hughes, B. R. Oxidation of biogenic and water-soluble compounds in aqueous and organic aerosol droplets by ozone: a kinetic and product analysis approach using laser Raman tweezers. *Faraday Discuss* **2008**, *137*, 173–92; discussion 193–204.

(19) Pope, F. D.; Gallimore, P. J.; Fuller, S. J.; Cox, R. A.; Kalberer, M. Ozonolysis of Maleic Acid Aerosols: Effect upon Aerosol Hygroscopicity, Phase and Mass. *Environ Sci Technol* **2010**, *44*, 6656–6660.

(20) Chan, L. P.; Chan, C. K. Roles of the Phase State and Water Content in Ozonolysis of Internal Mixtures of Maleic Acid and Ammonium Sulfate Particles. *Aerosol Sci Technol* **2012**, *46*, 781–793.

(21) Dennis-Smither, B. J.; Marshall, F. H.; Miles, R. E.; Preston, T. C.; Reid, J. P. Volatility and oxidative aging of aqueous maleic acid aerosol droplets and the dependence on relative humidity. *J Phys Chem A* **2014**, *118*, 5680–91.

(22) Hunt, O. R.; Ward, A. D.; King, M. D. Heterogeneous oxidation of nitrite anion by gas-phase ozone in an aqueous droplet levitated by laser tweezers (optical trap): is there any evidence for enhanced surface reaction? *Phys Chem Chem Phys* **2015**, *17*, 2734–2741.

(23) Brotton, S. J.; Kaiser, R. I. Controlled Chemistry via Contactless Manipulation and Merging of Droplets in an Acoustic Levitator. *Anal Chem* **2020**, *92*, 8371–8377.

(24) Noble, C. A.; Prather, K. A. Real-time single particle mass spectrometry: A historical review of a quarter century of the chemical analysis of aerosols. *Mass Spectrom Rev* **2000**, *19*, 248–274.

(25) Pratt, K. A.; Prather, K. A. Mass spectrometry of atmospheric aerosols–recent developments and applications. Part II: On-line mass spectrometry techniques. *Mass Spectrom Rev* **2012**, *31*, 17–48.

(26) Leiterer, J.; Panne, U.; Thunemann, A. F.; Weidner, S. M. Container-less polymerization in acoustically levitated droplets: an analytical study by GPC and MALDI-TOF mass spectrometry. *Anal Methods* **2011**, *3*, 70–73.

(27) Stindt, A.; Albrecht, M.; Panne, U.; Riedel, J. CO2 laser ionization of acoustically levitated droplets. *Anal Bioanal Chem* **2013**, *405*, 7005–7010.

(28) Warschat, C.; Stindt, A.; Panne, U.; Riedel, J. Mass Spectrometry of Levitated Droplets by Thermally Unconfined Infrared-Laser Desorption. *Anal Chem* **2015**, *87*, 8323–8327.

(29) Crawford, E. A.; Esen, C.; Volmer, D. A. Real Time Monitoring of Containerless Microreactions in Acoustically Levitated Droplets via Ambient Ionization Mass Spectrometry. *Anal Chem* **2016**, *88*, 8396–8403.

(30) Mu, C.; Wang, J.; Barraza, K. M.; Zhang, X.; Beauchamp, J. L. Mass Spectrometric Study of Acoustically Levitated Droplets Illuminates Molecular-Level Mechanism of Photodynamic Therapy for Cancer involving Lipid Oxidation. *Angew Chem Int Ed* **2019**, *58*, 8082–8086.

(31) Zhang, X.; Barraza, K. M.; Beauchamp, J. L. Cholesterol provides non-sacrificial protection of membrane lipids from chemical damage at air-water interface. *Proc Natl Acad Sci USA* **2018**, *115*, 3255–3260.

(32) Wozniak, M.; Derkachov, G.; Kolwas, K.; Archer, J.; Wojciechowski, T.; Jakubczyk, D.; Kolwas, M. Formation of Highly Ordered Spherical Aggregates from Drying Microdroplets of Colloidal Suspension. *Langmuir* **2015**, *31*, 7860–7868.

(33) Hart, M. B.; Sivaprakasam, V.; Eversole, J. D.; Johnson, L. J.; Czege, J. Optical measurements from single levitated particles using a linear electrodynamic quadrupole trap. *Appl Opt* **2015**, *54*, F174–F181.

(34) Bogan, M. J.; Agnes, G. R. MALDI-TOF-MS analysis of droplets prepared in an electrodynamic balance: "Wall-less" sample preparation. *Anal Chem* **2002**, *74*, 489–496.

(35) Haddrell, A. E.; Feng, X.; Nassar, R.; Bogan, M. J.; Agnes, G. R. Off-line LDI-TOF-MS monitoring of simultaneous inorganic and organic reactions on particles levitated in a laboratory environment. *J Aerosol Sci* **2005**, *36*, 521–533.

(36) Tracey, P. J.; Vaughn, B. S.; Roberts, B. J.; Poad, B. L. J.; Trevitt, A. J. Rapid Profiling of Laser-Induced Photochemistry in Single Microdroplets Using Mass Spectrometry. *Anal Chem* **2014**, *86*, 2895–2899.

(37) Kaur Kohli, R.; Davies, J. F. Paper Spray Mass Spectrometry for the Analysis of Picoliter Droplets. *Analyst* **2020**, *145*, 2639–2648.

(38) Birdsall, A. W.; Krieger, U. K.; Keutsch, F. N. Electrodynamic balance-mass spectrometry of single particles as a new platform for atmospheric chemistry research. *Atmos Meas Tech* **2018**, *11*, 33–47.

(39) Birdsall, A. W.; Hensley, J. C.; Kotowitz, P. S.; Huisman, A. J.; Keutsch, F. N. Single-particle experiments measuring humidity and inorganic salt effects on gas-particle partitioning of butenedial. *Atmos Chem Phys* **2019**, *19*, 14195–14209.

(40) Jacobs, M. I.; Davies, J. F.; Lee, L.; Davis, R. D.; Houle, F.; Wilson, K. R. Exploring Chemistry in Microcompartments Using Guided Droplet Collisions in a Branched Quadrupole Trap Coupled to a Single Droplet, Paper Spray Mass Spectrometer. *Anal Chem* **2017**, *89*, 12511–12519.

(41) Davies, J. F. Mass, Charge and Radius of Droplets in a Linear Quadrupole Electrodynamic Balance. *Aerosol Sci Technol* **2019**, 1–29.

(42) Davies, J. F.; Haddrell, A. E.; Reid, J. P. Time-Resolved Measurements of the Evapo-

ration of Volatile Components from Single Aerosol Droplets. *Aerosol Sci Technol* **2012**, *46*, 666–677.

(43) Espy, R. D.; Muliadi, A. R.; Ouyang, Z.; Cooks, R. G. Spray mechanism in paper spray ionization. *Int J Mass Spectrom* **2012**, *325-327*, 167–171.

(44) McBride, E. M.; Mach, P. M.; Dhummakupt, E. S.; Dowling, S.; Carmany, D. O.; Demond, P. S.; Rizzo, G.; Manicke, N. E.; Glaros, T. Paper spray ionization: Applications and perspectives. *Trends Anal Chem* **2019**, *118*, 722–730.

(45) Cody, R.; Laramee, J.; Durst, H. Versatile New Ion Source for the Analysis of Materials in Open Air under Ambient Conditions. *Anal Chem* **2005**, *77*, 2297–2302.

(46) Gross, J. H. Direct analysis in real time–a critical review on DART-MS. *Anal Bioanal Chem* **2014**, *406*, 63–80.

(47) Zhang, Z.; Xu, W.; Manicke, N. E.; Cooks, R. G.; Ouyang, Z. Silica coated paper substrate for paper-spray analysis of therapeutic drugs in dried blood spots. *Anal Chem* **2012**, *84*, 931–8.

(48) Yang, Q.; Wang, H.; Maas, J. D.; Chappell, W. J.; Manicke, N. E.; Cooks, R. G.; Ouyang, Z. Paper spray ionization devices for direct, biomedical analysis using mass spectrometry. *Int J Mass Spectrom* **2012**, *312*, 201–207.

(49) Vandergrift, G. W.; Hessels, A. J.; Palaty, J.; Krogh, E. T.; Gill, C. G. Paper spray mass spectrometry for the direct, semi-quantitative measurement of fentanyl and norfentanyl in complex matrices. *Clin Biochem* **2018**, *54*, 106–111.

(50) De Silva, I. W.; Converse, D. T.; Juel, L. A.; Verbeck, G. F. A comparative study of microporous polyolefin silica-based paper and cellulose paper substrates utilizing paper spray-mass spectrometry in drug analysis. *Anal Methods* **2019**, *11*, 3066–3072.

(51) Skaggs, C.; Kirkpatrick, L.; Wichert, W. R. A.; Skaggs, N.; Manicke, N. E. A statistical approach to optimizing paper spray mass spectrometry parameters. *Rapid Commun Mass Spectrom* **2020**, *34*, e8601.

(52) Upton, K. T.; Schilling, K. A.; Beauchamp, J. L. Easily fabricated ion source for characterizing mixtures of organic compounds by direct analysis in real time mass spectrometry. *Anal Methods* **2017**, *9*, 5065–5074.

(53) Shelley, J. T.; Wiley, J. S.; Chan, G. C.; Schilling, G. D.; Ray, S. J.; Hieftje, G. M. Characterization of direct-current atmospheric-pressure discharges useful for ambient desorption/ionization mass spectrometry. *J Am Soc Mass Spectrom* **2009**, *20*, 837–44.

(54) Zuend, A.; Marcolli, C.; Booth, A. M.; Lienhard, D. M.; Soonsin, V.; Krieger, U. K.; Topping, D. O.; McFiggans, G.; Peter, T.; Seinfeld, J. H. New and extended parameterization of the thermodynamic model AIOMFAC: calculation of activity coefficients for organic-inorganic mixtures containing carboxyl, hydroxyl, carbonyl, ether, ester, alkenyl, alkyl, and aromatic functional groups. *Atmos Chem Phys* **2011**, *11*, 9155–9206.

(55) McKenna, J.; Dhummakupt, E. S.; Connell, T.; Demond, P. S.; Miller, D. B.; Michael Nilles, J.; Manicke, N. E.; Glaros, T. Detection of chemical warfare agent simulants and hydrolysis products in biological samples by paper spray mass spectrometry. *Analyst* **2017**, *142*, 1442–1451.

(56) Liu, J.; Wang, H.; Manicke, N. E.; Lin, J.-M.; Cooks, R. G.; Ouyang, Z. Development, Characterization, and Application of Paper Spray Ionization. *Anal Chem* **2010**, *82*, 2463–2471.

(57) Cody, R. Observation of Molecular Ions and Analysis of Nonpolar Compounds with the Direct Analysis in Real Time Ion Source. *Anal Chem* **2009**, *81*, 1101–1107.

(58) Newsome, G. A.; Ackerman, L. K.; Johnson, K. J. Humidity affects relative ion abundance in direct analysis in real time mass spectrometry of hexamethylene triperoxide diamine. *Anal Chem* **2014**, *86*, 11977–80.

(59) Newsome, G. A.; Ackerman, L. K.; Johnson, K. J. Humidity Effects on Fragmentation in Plasma-Based Ambient Ionization Sources. *J Am Soc Mass Spectrom* **2016**, *27*, 135–43.

(60) de Gouw, J.; Warneke, C. Measurements of volatile organic compounds in the earth's atmosphere using proton-transfer-reaction mass spectrometry. *Mass Spectrom Rev* **2007**, *26*, 223–57.

(61) Lee, B. H.; Lopez-Hilfiker, F. D.; Mohr, C.; Kurten, T.; Worsnop, D. R.; Thornton, J. A. An Iodide-Adduct High-Resolution Time-of-Flight Chemical-Ionization Mass Spectrometer: Application to Atmospheric Inorganic and Organic Compounds. *Environ Sci Technol* **2014**, *48*, 6309–6317.

(62) Brophy, P.; Farmer, D. K. Clustering, methodology, and mechanistic insights into acetate chemical ionization using high-resolution time-of-flight mass spectrometry. *Atmos Meas Tech* **2016**, *9*, 3969–3986.

(63) Novak, G. A.; Vermeuel, M. P.; Bertram, T. H. Simultaneous detection of ozone and nitrogen dioxide by oxygen anion chemical ionization mass spectrometry: a fast-time-response sensor suitable for eddy covariance measurements. *Atmos Meas Tech* **2020**, *13*, 1887–1907.

(64) Tanner, S.; Mackay, G.; Bohme, D. An experimental study of the reactivity of the hydroxide anion in the gas phase at room temperature, and its perturbation by hydration. *Can J Chem* **1981**, *59*, 1615.

(65) Song, L.; Dykstra, A. B.; Yao, H.; Bartmess, J. E. Ionization mechanism of negative

ion-direct analysis in real time: a comparative study with negative ion-atmospheric pressure photoionization. *J Am Soc Mass Spectrom* **2009**, *20*, 42–50.

(66) Custer, T. G.; Kato, S.; Fall, R.; Bierbaum, V. M. Negative ion mass spectrometry and the detection of carbonyls and HCN from clover. *Geophys Res Lett* **2000**, *27*, 3849–3852.

(67) Ghislain, M.; Costarramone, N.; Sotiropoulos, J. M.; Pigot, T.; Van Den Berg, R.; Lacombe, S.; Le Bechec, M. Direct analysis of aldehydes and carboxylic acids in the gas phase by negative ionization selected ion flow tube mass spectrometry: Quantification and modelling of ion-molecule reactions. *Rapid Commun Mass Spectrom* **2019**, *33*, 1623–1634.

(68) Shelley, J. T.; Hieftje, G. M. Ionization matrix effects in plasma-based ambient mass spectrometry sources. *J Anal At Spectrom* **2010**, *25*.

(69) Cappa, C. D.; Lovejoy, E. R.; Ravishankara, A. R. Evidence for liquid-like and nonideal behavior of a mixture of organic aerosol components. *Proc Natl Acad Sci USA* **2008**, *105*, 18687–91.

(70) Bilde, M. et al. Saturation vapor pressures and transition enthalpies of low-volatility organic molecules of atmospheric relevance: from dicarboxylic acids to complex mixtures. *Chem Rev* **2015**, *115*, 4115–56.

(71) Smith, J. D.; Kroll, J. H.; Cappa, C.; Che, D. L.; Liu, C. L.; Ahmed, M.; Leone, S. R.; Worsnop, D.; Wilson, K. R. The heterogeneous reaction of hydroxyl radicals with submicron squalane particles: a model system for understanding the oxidative aging of ambient aerosols. *Atmos Chem Phys* **2009**, *9*, 3209–3222.

(72) Najera, J. J.; Percival, C. J.; Horn, A. B. Kinetic studies of the heterogeneous oxidation of maleic and fumaric acid aerosols by ozone under conditions of high relative humidity. *Phys Chem Chem Phys* **2010**, *12*, 11417–27.

(73) Gallimore, P. J.; Achakulwisut, P.; Pope, F. D.; Davies, J. F.; Spring, D. R.; Kalberer, M. Importance of relative humidity in the oxidative ageing of organic aerosols: case study of the ozonolysis of maleic acid aerosol. *Atmos Chem Phys* **2011**, *11*, 12181–12195.

Graphical TOC Entry